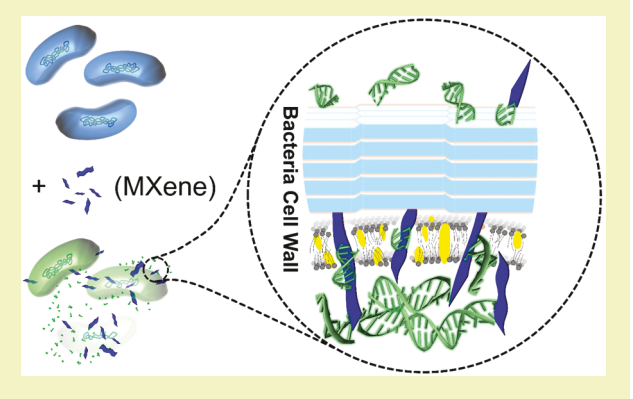


# Antimicrobial Mode-of-Action of Colloidal Ti<sub>3</sub>C<sub>2</sub>T<sub>x</sub> MXene **Nanosheets**

Ahmad Arabi Shamsabadi,<sup>†,¶</sup>® Mohammad Sharifian Gh.,<sup>‡,¶</sup>® Babak Anasori,<sup>§</sup>® and Masoud Soroush\*,<sup>†</sup>

Supporting Information

ABSTRACT: Antibacterial properties of two-dimensional (2D) nanomaterials are of great interest in fields such as environmental engineering, biomedical engineering, and medicine. Ti<sub>3</sub>C<sub>2</sub>T<sub>x</sub> MXene, a novel 2D nanomaterial, has been reported to have excellent antibacterial activity against both Gram-negative and Gram-positive bacteria. This paper presents the first study aimed at determining the primary antibacterial mode-of-action of the MXene. We studied the antibacterial properties of MXene nanosheets with lateral sizes of 0.09, 0.35, 0.57, and 4.40  $\mu$ m against Escherichia coli and Bacillus subtilis bacteria for 3 and 8 h in the dark. Quantitative analyses of bacteria species performed with complementary techniques, fluorescence imaging, and flow cytometry confirmed that the antibacterial activity of the MXene nanosheets is both size- and exposure-time-dependent. Smaller



nanosheets showed higher antibacterial activities against both bacteria. For the first time, we applied broth microdilution assay to determine whether direct physical interactions between the MXene nanosheets and bacteria cells play a part in antibacterial properties of the nanosheets. Growth kinetics measurements evidently indicate that direct physical interactions between the sharp edges of the nanosheets and bacteria membrane surfaces play a crucial part in antibacterial properties of the nanosheets. The MXene nanosheets were found to damage the bacterial cells significantly in less than 3 h, leading to the release of bacteria DNA from the cytosol followed by bacteria cell dispersion. These results point to the great potential of MXene-based antibacterial products for water treatment, medical, and biomedical applications.

KEYWORDS: MXene, 2D nanomaterials, antibacterial, mode-of-action, bacterial membranes, DNA release

### **■** INTRODUCTION

Antimicrobial resistance lowers the effectiveness of bactericidal compounds. Because of this ongoing problem along with the antimicrobial side effects, there is a strong demand for the development of innovative compounds that can target microbial pathogens selectively and efficiently. 1-7 To this end, nanomaterials with biocidal properties (e.g., silver-based nanomaterials)8-15 have been studied for environmental and biomedical applications such as wound infection healing, 16-19 water treatment, <sup>20,21</sup> textile fabrics, <sup>22</sup> and foodstuffs. <sup>23,24</sup>

Because of their outstanding antimicrobial properties, twodimensional (2D) nanomaterials have received a lot of attention. <sup>25-31</sup> Among 2D nanomaterials, antibacterial properties of graphene-based nanomaterials have been studied most. 27,32-40 In addition to graphene-based materials, molybdenum disulfide (MoS<sub>2</sub>) nanosheets have displayed excellent antibacterial activity. <sup>16,17,25,41–43</sup> Specifically, functionalized exfoliated MoS2 have exhibited highly effective bacterial growth inhibition against Staphylococcus aureus and

Pseudomonas aeruginosa, in which oxidative stress and fast membrane depolarization were found to be the most probable bactericidal mechanisms. 44 A better understanding of the primary antimicrobial mode-of-action (MoA) of a nanomaterial allows for tailoring the antibacterial activity of the nanomaterial. Previous studies compared various parameters that may play a part in potential antimicrobial properties of graphene-based nanomaterials. 27,32-37,45 For example, oxygencontaining functional groups of graphene oxide (GO) contribute significantly to the antibacterial activity of GO.<sup>34–37</sup>

In contrast to graphene-based nanomaterials, so far there have been only two studies on the biocidal activity of Ti<sub>3</sub>C<sub>2</sub>T<sub>w</sub> MXene nanosheets. 46,47 It was speculated that sharp edges of MXene nanosheets damage bacterial membranes, resulting in

Received: August 3, 2018 Revised: September 18, 2018 Published: October 15, 2018

<sup>&</sup>lt;sup>†</sup>Department of Chemical and Biological Engineering, Drexel University, Philadelphia, Pennsylvania 19104, United States

<sup>&</sup>lt;sup>‡</sup>Department of Chemistry, Temple University, Philadelphia, Pennsylvania 19122, United States

Department of Materials Science and Engineering, and A. J. Drexel Nanomaterials Institute, Drexel University, Philadelphia, Pennsylvania 19104, United States

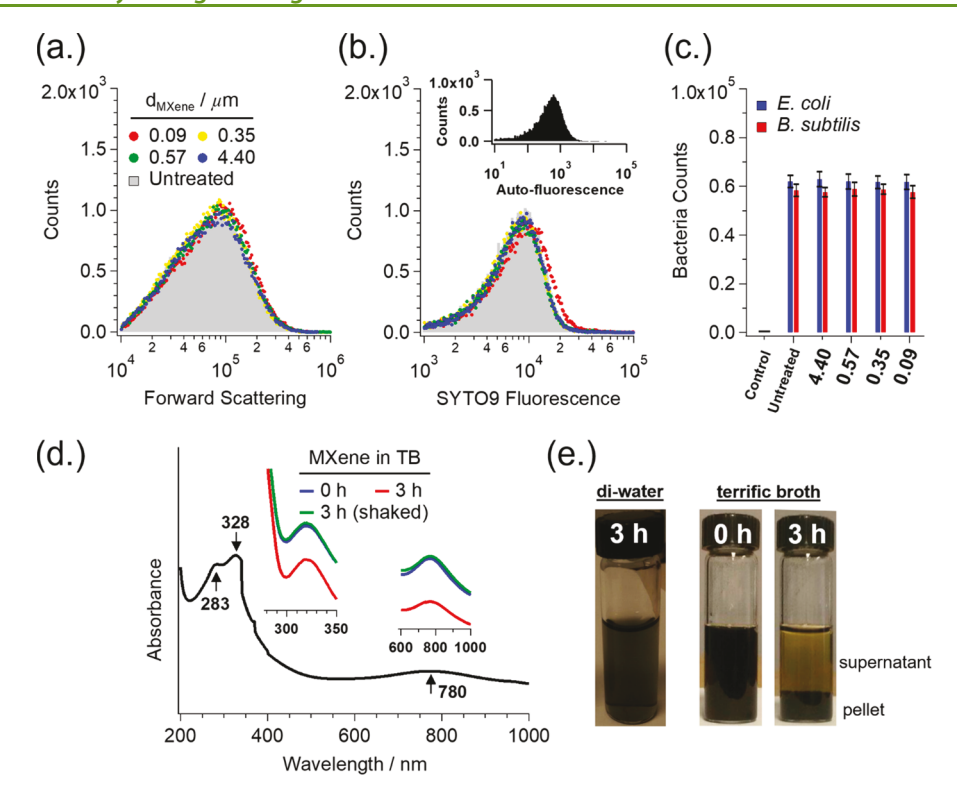


Figure 1. MXene precipitation in TB culture media induces its antimicrobial properties. (a-c) FC analysis of cultured B. subtilis and E. coli bacteria in TB media for untreated and treated samples with  $100~\mu g/mL$  of  $Ti_3C_2T_x$  MXene nanosheets of various sizes. The FSC (a) and SYTO9 fluorescence (b) histograms depict the populations of detected particles (i.e., bacteria and nanosheets) and real bacteria cells, respectively. The histograms of untreated bacteria are shown with the gray background signals. The inset in (b) represents the autofluorescence histogram of unstained bacteria for comparison. The numbers of cultured bacteria cells from (b) are shown in (c) for both bacteria strains. Each error bar was obtained from three independent experiments on each bacteria strain. (d) UV–vis spectra of  $0.09-\mu m$  MXene suspensions in deionized (DI) water (black spectra) and TB solution (colored spectra) after 0 and 3 h. (e) MXene suspensions are stable in DI water but precipitated in TB media after 3 h.

bacteria death, <sup>47</sup> and smaller nanosheets may infuse into the microorganisms via endocytosis or direct physical penetration.

This work was aimed to study the primary antibacterial MoA of Ti<sub>3</sub>C<sub>2</sub>T<sub>r</sub> MXene nanosheets against both Gram-negative and Gram-positive bacteria. Understanding the MoA will allow for developing minimally toxic antibacterial agents for medical and biomedical purposes. Our hypothesis was that the bacterial cell wall is damaged by the sharp edges of the MXene, leading to the loss of membrane integrity and eventually bacteria death. To evaluate our hypothesis, the antibacterial activity of 100 μg/mL colloidal solutions of Ti<sub>3</sub>C<sub>2</sub>T<sub>r</sub> MXene nanosheets with average lateral sizes of 0.09, 0.35, 0.57, and 4.40  $\mu m$  was evaluated. If sharp edges of the nanosheets contribute significantly to damaging the membrane integrity of bacteria, then smaller nanosheets should have higher antibacterial activity. We evaluated the antibacterial activity against Bacillus (B.) subtilis and Escherichia (E.) coli. To ensure that only the MXene contributed to the observed antibacterial activity, the bacteria was incubated with the nanosheets in the dark, and the experiments were carried out at conditions that minimized the contributions of factors such as osmotic shock and mechanical force. The incubation in the dark minimized contributions of oxidative stress (i.e., mainly reactive oxygen species (ROS)dependent oxidative stress) to the observed antibacterial activity. 48,49 In this study, we applied more quantitative techniques and approaches than in previous studies on MXenes and other 2D materials, to shed light on the MoA. We applied broth microdilution assay<sup>50</sup> to determine whether

direct physical interactions between the Ti<sub>3</sub>C<sub>2</sub>T<sub>x</sub> MXene nanosheets and the bacteria cells play a part in antibacterial properties of the nanosheets. Additionally, to characterize the antibacterial properties of Ti<sub>3</sub>C<sub>2</sub>T<sub>x</sub> MXene in an effectively quantitative manner, we used the flow cytometry (FC) technique, 51-53 in which SYTO9 fluorescence enhancement in SYTO9-DNA intercalation was exploited to remove the interference of the nanosheets from bacteria cells in the FC measurements (i.e., SYTO9 is a green fluorescent nucleic acid stain for staining bacteria cells). Fluorescence imaging (FI) was also used as a complementary technique to visually confirm the FC results. Our results indicated that the antibacterial activity of the MXene nanosheets are both size- and time-dependent; that is, smaller sizes of the nanosheets result in the release of bacteria cytoplasmic DNA and eventually dispersion of the bacteria envelope.

# ■ RESULTS AND DISCUSSION

# Physical Interactions between MXene and Bacteria.

Bacteria growth kinetics was monitored using optical density (OD) measurements of bacteria suspensions at 600 nm (i.e.,  $OD_{600} = 0.1$  is equivalent to  $10^8$  cfu/ml)<sup>54–60</sup> to examine antimicrobial properties and the dosage of various 2D nanomaterials (including MXene nanosheets) against the bacteria strains. <sup>46,47,61–65</sup> In these studies, bacteria were allowed to grow in terrific broth (TB) culture media in the absence and the presence of 2D nanomaterials. Here, we apply broth microdilution assay<sup>50</sup> to examine inhibitory properties of

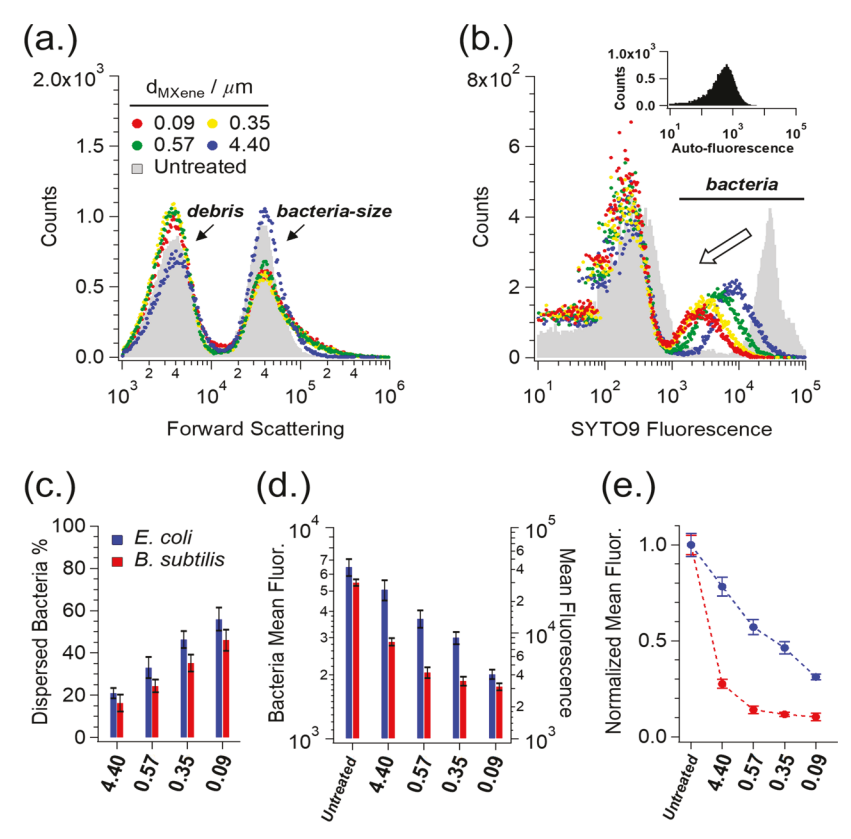


Figure 2. Antibacterial activity of various sizes of  $T_{i_3}C_2T_x$  MXene nanosheets against *B. subtilis* and *E. coli* investigated via FC analyses. (a) FSC histogram of bacteria treated and untreated with  $100 \,\mu g/mL$  MXene nanosheets for 3 h in the dark. Debris and bacteria-size populations are shown by arrows. (b) SYTO9 fluorescence histogram depict the populations of bacteria cells in (a), where histograms of untreated bacteria and the autofluorescence histogram of unstained bacteria are shown by the gray background and the inset, respectively. The percentage of MXene-induced dispersed bacteria and the bacteria mean fluorescence are quantified and depicted in (c) and (d), respectively. The bacteria mean fluorescence signals are normalized to untreated samples and depicted in (e). Each error bar was obtained from three independent experiments on each bacteria strain. The lines between points in (e) are not fitted lines; they were added to show the trends.

MXene nanosheets against the growth of *B. subtilis* and *E. coli*. Each bacteria strain with a final density of  $10^8$  cfu/ml in TB culture media was treated with  $100~\mu g/mL$  of 0.09, 0.35, 0.57, and  $4.40~\mu m$  wide  $Ti_3C_2T_x$  MXene nanosheets. The strain was then grown aerobically at 37 °C at 150 rpm for ~18 h. To quantify the cultivated bacteria, we performed the FC measurements of the bacteria/MXene suspensions. To reduce the effect of debris in our FC analysis, we set thresholds of 10~000 for forward angle scatting (FSC) and 100 for side angle scattering (SSC) signals (see Materials and Methods). FSC histograms depict the particles size distributions along with the total number of the particles detected in the population-of-interest.

As depicted in Figure 1a, for a constant volume of the analyzed samples (i.e.,  $10~\mu L$ ), FSC histograms of the suspensions are totally conserved for both bacteria strains regardless of  $Ti_3C_2T_x$  MXene nanosheets lateral size. Indeed, various sizes of MXene nanosheets did not induce any significant changes in the total number of the particles and their size distributions in treated bacteria samples. We should note that although the FSC histograms of the samples provide information about the population of the bacteria-size particles, it is unable to distinguish bacteria from the MXene nanosheets in the FC measurements. To eliminate any interferences from the nanosheets in our FC analysis, we incubated the treated and untreated bacteria samples with SYTO9. SYTO9 exhibits a fluorescence enhancement of  $\sim$ 30-fold upon intercalation into

the DNA double-strand. Because bacteria DNA molecules were found exclusively inside the cytoplasmic region, for SYTO9 to interact with the bacteria DNA molecules, they have to pass through the cytoplasmic membrane (CM) of bacteria. Also, SYTO9 easily cross the bacteria CM, which results in a green fluorescence enhancement. Given that Ti<sub>3</sub>C<sub>2</sub>T<sub>x</sub> MXene nanosheets do not produce fluorescence enhancement with the SYTO9 molecule (see SI for details), intercalation of SYTO9 with bacterial DNA can be exploited to differentiate bacteria from the MXene nanosheets in a particular population-ofinterest. Figure 1b exhibits the histogram of the SYTO9 fluorescence signals from Figure 1a. Neither the position nor the height of the fluorescence histograms are affected by the MXene-treated bacteria strains. We note that the slightly shifted histograms for the 0.09-\mu MXene-treated samples are almost certainly due to the lower optical density of the samples, which allowed more fluorescence signals to reach the FC detector. Figure 1c depicts the bacteria counts resulted from the histogram in Figure 1b for both bacteria strains. These results show that even a high density of 100  $\mu$ g/mL MXene nanosheets cannot induce any significant changes in bacteria growth over ~18 h treatment. We also note that the MXene nanosheets do not interfere with bacteria cells in FC measurements. Of significance, Figure S1 exhibits SYTO9 fluorescence histogram of various sizes of MXene nanosheets (no bacteria cells present) stained with 5  $\mu$ M SYTO9 in which the fluorescence signals of the MXene nanosheets are completely apart from the one from untreated bacteria sample stained with 5  $\mu$ M SYTO9.

As shown in Figure 1a—c, there are no substantial differences in the total counts of untreated and MXene-treated bacteria samples, indicating that MXene has no significant effect on the bacteria growth. MXene precipitation in the TB media induces the peaks intensities, while no shifts are observed in the peak wavelengths. One hypothesis is that Ti<sub>3</sub>C<sub>2</sub>T<sub>x</sub> MXene nanosheets precipitate in TB media, which decreases the probability of physical interaction between the nanosheets and bacteria surfaces. To test this hypothesis, we recorded the UV-vis spectra of 0.09-um MXene suspensions in DI water and in TB media after 0 and 3 h. As depicted in Figure 1d, MXene precipitation in TB media causes a decrease in the MXene peak intensities (i.e., 328 and 780 nm) after 3 h exposure. However, shaking the suspension resulted in the recovery of the peak intensities (also see Figure 1e for the MXene suspensions prepared in DI water and TB media). We note that no shift was observed in the peak wavelengths indicating that TB did not produce any chemical changes in the MXene nanosheets even after 3 h exposure (neither did PBS; see Figure S2). These results suggest that Ti<sub>3</sub>C<sub>2</sub>T<sub>x</sub> MXene precipitation in a TB culture media significantly inhibits its antibacterial properties, agreeing with the conclusions from Figure 1a-c that physical interactions between the MXene and bacteria is crucial in antibacterial properties of the nanosheets. As this precipitation can create significant uncertainty in OD measurements, broth microdilution assay is recommended for investigating whether physical interactions between nanomaterials and bacteria cell surfaces contribute significantly to antibacterial properties of nanomaterials.

Size-Dependent Antibacterial Activity of the MXene. Figure 2 exhibits the FC analysis of bacteria samples, which characterizes the antibacterial activity of different sizes of MXene nanosheets against *B. subtilis* and *E. coli*. Bacteria suspensions with a density of  $10^8$  cfu/ml were treated with 100  $\mu$ g/mL colloidal solutions of the MXene nanosheets with average lateral sizes of 0.09, 0.35, 0.57, and 4.40  $\mu$ m for 3 h in the dark; this implies that the ratio of the nanosheets to bacteria was about 1 pg/cfu. To minimize the contributions of oxidative stress (which is mainly due to ROS-dependent oxidative stress) to the observer antibacterial activity of  $Ti_3C_2T_{xy}$  we incubated the bacteria with MXene nanosheets in the dark.

To investigate the probable production of debris in our samples, we set the lower thresholds of 1000 for FSC and 10 for SSC signals (see Materials and Methods in the SI). As shown in Figure 2a, there are two distinct populations in the FSC histogram, the low FSC (i.e., debris) and high FSC (i.e., bacteria-size) populations. The population of untreated bacteria is shown by a background gray histogram. Significantly, 4.40-µm MXene nanosheets did not make significant changes in the two populations. However, the other three sizes of the nanosheets decreased the live bacteria population by ~40% and simultaneously increased the debris population by ~25%. As discussed before, we used SYTO9 to differentiate bacteria from the MXene nanosheets in the FC measurements. Figure 2b exhibits the histogram of the SYTO9 fluorescence signals for the untreated and treated bacteria samples from Figure 2a. As depicted, there are two distinct populations. The population with fluorescence of <10<sup>3</sup> corresponds to the stained debris and the autofluorescence of the biological molecules in the bacteria cytosol. The

population with the fluorescence of >10³ corresponds to the stained bacteria populations. Given that the FC experiments were performed under constant-volume samples (i.e., 10  $\mu$ L), the >10³ population represents the relative number of bacteria in treated versus untreated samples. The trend is marked by an arrow in Figure 2b, where decreasing the average lateral size of Ti<sub>3</sub>C<sub>2</sub>T<sub>x</sub> sheets, from 0.09 to 4.40  $\mu$ m, leads to a significant decrease in both bacteria counts and SYTO9 fluorescence intensities.

The SYTO9 fluorescence histograms were used to quantify the number of dispersed bacteria in MXene-treated samples. As depicted in Figure 2c, in both B. subtilis and E. coli samples, a significant percentage of bacteria cells were dispersed after treatment with the nanosheets, and smaller sizes of the nanosheets produced higher percentages of dispersed bacteria. Of significance, a 3-h treatment of E. coli and B. subtilis with 0.09, 0.35, 0.57, and 4.40  $\mu$ m nanosheets resulted in the dispersion of ~50%, 40%, 30%, and 20% of the bacteria populations, respectively. Our results show that smaller lateral sizes of the Ti<sub>3</sub>C<sub>2</sub>T<sub>x</sub> nanosheets leads to more damage to the bacteria envelope.

Figure 2d represents a semiquantitative analysis of the amount of bacterial cytoplasmic DNA in untreated and MXene-treated samples. The mean fluorescence of the bacteria population was calculated from the SYTO9 fluorescence histograms in Figure 2b. Bacteria populations treated with smaller sizes of the Ti<sub>3</sub>C<sub>2</sub>T<sub>x</sub> MXene nanosheets contained less amount of stained cytoplasmic DNA. The smaller MXene nanosheets had higher antibacterial activity against both bacteria strains, especially against B. subtilis. Given that the same amount of MXene nanosheets of various sizes were applied to the bacteria samples, more nanosheets per bacteria cells are expected for smaller sizes. In other words, bacteria cells experience more sharp edges of the smaller than larger nanosheets. Moreover, for smaller sizes of the nanomaterial, there is a higher probability of getting into the cytosol and damaging the cytoplasmic components, mainly the DNA. This suggests that the MXene-treatment resulted in the release of DNA from the bacterial cytosol. To highlight the decrease in the concentration of the cytoplasmic DNA, the mean fluorescence signals were normalized to the corresponding signal for untreated bacteria samples (Figure 2e). The release of DNA from both B. subtilis and E. coli increased significantly, as the nanosheet size decreased. Three-hour treatments of E. coli with 0.09, 0.35, 0.57, and 4.40  $\mu$ m nanosheets decreased in the bacteria mean fluorescence intensity by ~70%, 55%, 40%, and 20%, respectively. These decreases were more significant for B. subtilis bacteria; 3 h treatment of B. subtilis with 0.09, 0.35, 0.57, and 4.40  $\mu$ m nanosheets decreased in the bacteria mean fluorescence intensity by ~92%, 90%, 85%, and 75%, respectively. MXene-induced damages to the bacteria envelope, which resulted in cytoplasmic DNA release and bacteria dispersion, were found to be nanosheet-size-dependent.

Stronger Size-Dependent Damages to Bacteria Envelope for Longer Exposures. As discussed in the previous sections, 0.09- $\mu$ m  $Ti_3C_2T_x$  MXene nanosheets significantly damaged both *B. subtilis* and *E. coli* bacteria, which resulted in the release of cytoplasmic DNA and eventually bacteria dispersion. To evaluate how the exposure time affects antibacterial properties of the nanosheets, we allowed bacteria samples to be in contact with the smallest lateral size MXene nanosheets used in this study (i.e., the 0.09- $\mu$ m lateral size nanosheets) for up to 8 h in the dark. Figure 3

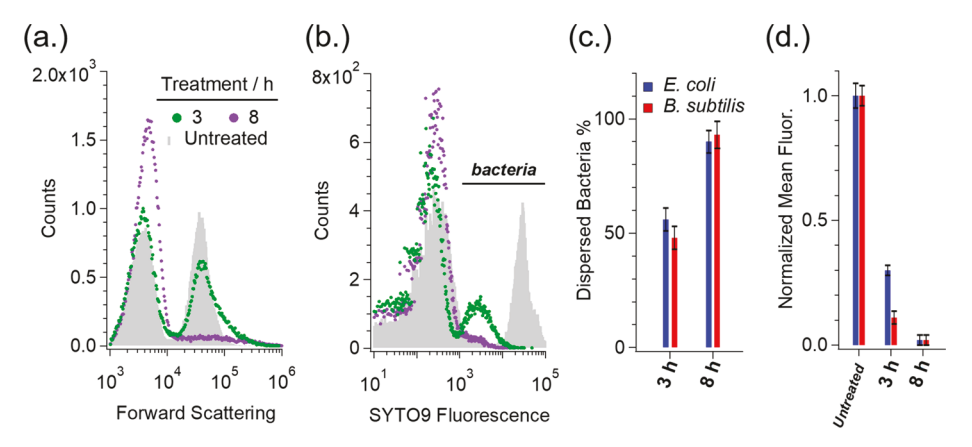


Figure 3. Antibacterial activity of 0.09- $\mu$ m Ti<sub>3</sub>C<sub>2</sub>T<sub>x</sub> MXene nanosheets against *B. subtilis* and *E. coli* investigated via FC analyses. FSC (a) and SYTO9 fluorescence (b) histograms of bacteria treated and untreated with 100  $\mu$ g/mL MXene nanosheets for 3 and 8 h in the dark. The fluorescent populations move to smaller counts and lower intensities for longer treatments, which are quantitatively analyzed in (c) and (d). As shown, the majority of the bacteria population was dispersed after 8 h treatment with 0.09- $\mu$ m MXene nanosheets. Each error bar was obtained from three independent experiments on each bacteria strain.

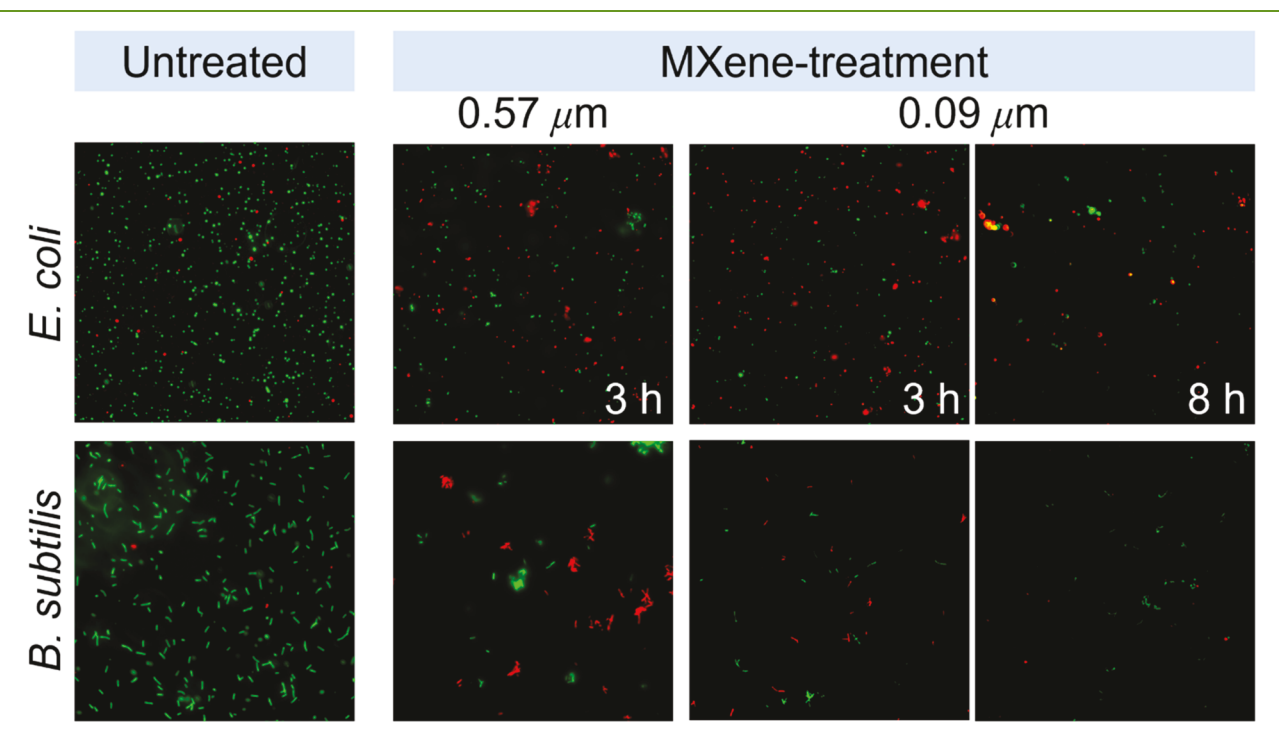


Figure 4. Antibacterial activity of 100  $\mu$ g/mL MXene nanosheets of 0.09- and 0.57- $\mu$ m sizes against *B. subtilis* and *E. coli* investigated by fluorescence imaging. The bacteria were treated with  $Ti_3C_2T_x$  MXene nanosheets for 3 or 8 h in the dark. As shown, the majority of bacteria population was dispersed after 8 h treatment with the 0.09- $\mu$ m MXene nanosheets.

depicts the FC analysis of *B. subtilis* and *E. coli* treated with 100  $\mu$ g/mL of the nanosheets for 3 and 8 h. Both FSC and SYTO9 fluorescence histograms (Figure 3a,b) clearly suggest that the majority of bacteria population was dispersed for the longer exposure time. Figure 3c exhibits the quantitate analysis of the results from Figure 3b. The treatment of *B. subtilis* and *E. coli* with 0.09- $\mu$ m MXene nanosheets for 8 h in the dark resulted in >90% dispersion of the bacteria samples. Moreover, Figure 3d shows that more than 95% of the DNA content were released from the bacteria cytosol. These results support the notion that smaller sizes of the nanosheets significantly damage the bacteria membranes, cause the DNA release, and eventually disperse bacteria cells.

To investigate these effects, we applied the FI technique, as a complementary approach to the FC analysis, to measure the viability of bacteria cells in MXene-treated samples. Similar to SYTO9, propidium iodide (PI) exhibits a fluorescence enhancement upon intercalation into the DNA double-strand. In contrast to the SYTO9 molecule, the PI molecule does not cross the CM of live bacteria cells, and therefore, no fluorescence enhancement is observed. Nevertheless, bacteria with disrupted membranes exhibit an induced permeability enhancement of the CM, which results in the uptake of PI molecules into the cytoplasmic region followed by fluorescence enhancement. The use of both fluorescent molecules allowed us to estimate the dead/live ratio in bacteria samples (i.e., SYTO9-stained and PI-stained cells are indicative

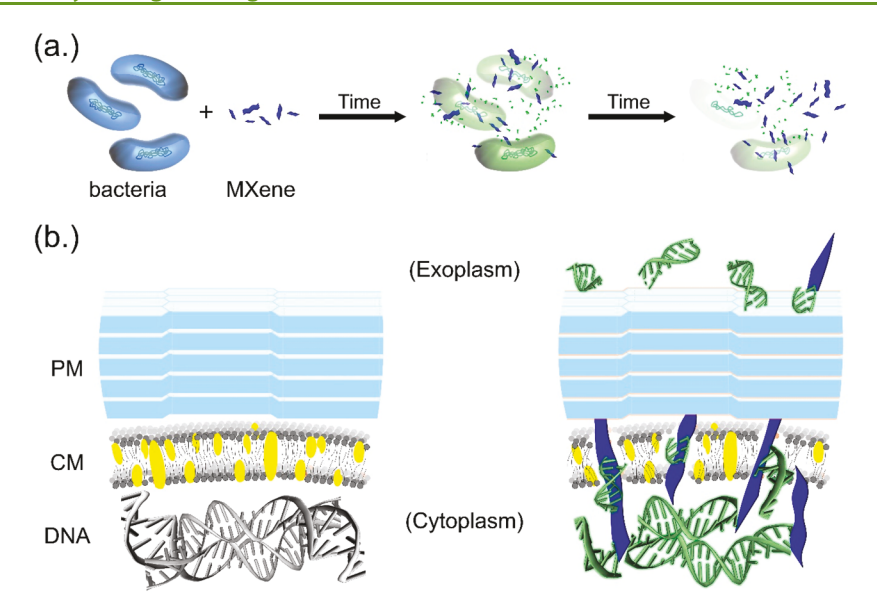


Figure 5. Schematic representation of our proposed antibacterial MoA of  $Ti_3C_2T_x$  MXene nanosheets. (a) Interactions of the nanosheets with bacteria cells result in the release of bacteria DNA and eventually bacteria dispersion. (b) MXene sharp nanosheets get into the bacteria cytoplasmic region by cutting the bacteria cell wall. PM and CM stand for peptidoglycan mesh and cytoplasmic membrane, respectively.

of live and dead bacteria, respectively). 51-53,70,71 Figure 4 depicts the antibacterial activity of 100 µg/mL Ti<sub>3</sub>C<sub>2</sub>T<sub>x</sub> MXene nanosheets of 0.09- and 0.57-µm sizes against B. subtilis and E. coli investigated by the FI, where the bacteria were treated with the nanosheets for 3 and 8 h in the dark. The number of dead bacteria (i.e., the PI-stained bacteria) in untreated samples were  $\sim 2-5\%$ . However, treatment of the bacteria with 0.57μm MXene for 3 h resulted in an obvious increase in the dead population in both bacteria samples. Moreover, the treatment of the bacteria with the smallest lateral size nanosheets (0.09μm MXene) resulted not only in higher populations of dead bacteria but also in less fluorescence intensities, supporting the notion that the smaller nanosheets caused the release of DNA from the bacteria cytosol. Notably, the treatment of the bacteria with 0.09-μm MXene for 8 h resulted in dispersing the majority of the population in both strains.

Proposed Inhibition Mechanism of Colloidal MXene Nanosheets. On the basis of our findings presented herein, we propose that Ti<sub>3</sub>C<sub>2</sub>T<sub>x</sub> MXene nanosheets with sharp edges get into the bacteria cytoplasmic region by cutting through the bacteria cell wall, resulting in the release of bacteria DNA and eventually bacteria dispersion. Figure 5 is a schematic representation of the proposed antibacterial MoA of the colloidal MXene nanosheets. As discussed in the previous sections, for the MXene nanosheets to show antibacterial properties against B. subtilis and E. coli, they should have direct physical contacts with the bacteria surfaces (see Figure 1). Furthermore, the FC and FI results (Figures 2-4) depict that the antibacterial activity of the MXene nanosheets is size and exposure-time dependent. Indeed, the smaller MXene flake sizes caused more damage to the cells especially for longer exposure times. Considering the average thickness of the bacteria cell walls (i.e., 20-50 nm), 54,72,73 the sharp (i.e.,  $\sim 1$ nm thick) edge of MXene flakes most probably cut through the bacteria membranes and reach the cytoplasmic DNA. Also, by reducing the MXene flakes lateral size, the number of sharp edges increases and make MXene flakes more effective in cutting bacteria membrane. During the first 3 h of the treatment with the nanosheets, the release of DNA from

bacteria cytosol was observed. However, for longer exposure times, significant damages in the bacteria cell wall resulted in the dispersion of bacteria population.

It is worth noting that our observations are in a good agreement with previous studies. For instance, Rasool et al. 47 detected the MXene-induced damages to the bacteria membranes using the scanning (SEM) and transmission electron microscopy (TEM). Their SEM imaging results pointed to the interactions of the MXene nanosheets (with the minimum concentration of 50  $\mu$ g/mL) with the bacteria surface, causing prevalent cell lysis indicated by a severe membrane disruption and cytoplasm leakage. Furthermore, their high-resolution TEM results demonstrated that the MXene nanosheets tightly adsorb around and enter into the bacteria cells, which eventually lowers intracellular densities of both bacteria species. 47

The isoelectric point of the bacteria surface has been reported to be in the range of 1.75–4.15 for Gram+ and 2.07–3.65 for Gram— bacteria species.  $^{74-76}$  At the pH of 7.3 of our study, both bacterial species should be repelled by the negatively charged  ${\rm Ti}_3{\rm C}_2{\rm T}_{\rm x}$  MXene nanosheets having a zeta potential of -31 mV. Hence, the bacterial surface charge should not contribute to the interactions of the MXene nanosheets with bacterial surfaces. However, the slightly more negative surface charge of Gram— bacterial may contribute to the higher resistance of Gram— species (e.g., *E. coli*) to the MXene nanosheets. The good agreement between our results and previous ones suggests that the MXene and other 2D nanomaterials (e.g., graphene family nanomaterials) act as nanoknives.  $^{27,32,37,42}$ 

Bacteria are prokaryotic, which means they do not contain a membrane-bound nucleus. Therefore, bacteria DNAs freely float in the cytosol.<sup>54</sup> As a result, any permeant molecule or compound that is able to pass across the bacteria cell walls may reach the freely floating DNAs as there is no other membrane barrier to pass through. Unlike previous reports, this work showed evidently the existence of interactions between MXene nanosheets and the bacteria DNA molecules. It is known that peptidoglycan mesh (PM) plays a crucial part in preserving the

integrity of bacteria cell walls by creating a turgor pressure of ~4 atm from the cytoplasmic space toward the exoplasmic region.<sup>54</sup> Therefore, any external stimulus (e.g., interaction with the nanomaterials) can lead to the loss of the bacterial membrane integrity 54,77 and/or the extraction of the lipid molecules from the membranes.<sup>78</sup> Our results suggest that interaction of the MXene nanosheets with the bacteria membrane surfaces results in reducing the integrity of the cell wall and eventually bacteria dispersion in both Gramnegative and Gram-positive species. We should note that because of similar structures of prokaryotic and eukaryotic cell (e.g., human cell) membranes, interactions between antibacterial and eukaryotic cells are always likely. 29,79-82 For instance, Jastrzebska et al.<sup>29</sup> have examined cytotoxicity of delaminated Ti<sub>3</sub>C<sub>2</sub> MXene against normal and cancerous cell lines in vitro. They have reported higher toxicity of the MXene against cancerous cells, which is thought to be due to the generation of ROS in the cells. Nevertheless, Nasrallah et al. 80 have reported that the MXene at concentrations of  $\leq 50 \mu g$ mL<sup>-1</sup> has no significant teratogenic effects on zebrafish embryos. Overall, understanding how 2D nanomaterials interact with bacteria membranes allows for developing minimally toxic antibacterial agents for medical and biomedical purposes. Specifically, the absence of the PM in the human cell membrane makes it a unique target for antibacterial. Therefore, any nanomaterial that primarily targets the PM, but not the plasma membrane, can be a great candidate for antibacterial applications.

## CONCLUSIONS

The antimicrobial MoA of Ti<sub>3</sub>C<sub>2</sub>T<sub>x</sub> MXene nanosheets was investigated via treating the bacteria samples (B. subtilis and E. coli) with 100 μg/mL colloidal solutions of the MXene nanosheets with average lateral sizes of 0.09, 0.35, 0.57, and 4.40  $\mu$ m. Broth microdilution assay was applied to examine inhibitory properties of the MXene nanosheets against the growth of B. subtilis and E. coli. This study indicated that direct physical interactions between the sharp edges of the nanosheets and bacteria membrane surfaces play a significant part in antibacterial properties of the nanosheets. In the FC analysis, the intercalation of the SYTO9 molecule with bacteria DNA was exploited to differentiate bacteria from the MXene nanosheets in a particular population-of-interest. The FC and FI results indicated that Ti<sub>3</sub>C<sub>2</sub>T<sub>x</sub> MXene nanosheets damage the bacterial cell wall significantly in less than 3 h, resulting in the release of bacteria DNA from the cytosol followed by the dispersion of the bacteria cells. This work showed that the antibacterial activity of the nanosheets is both size- and exposure-time-dependent. Of significance is that the treatment of B. subtilis and E. coli bacteria with 0.09-4.40 µm Ti<sub>3</sub>C<sub>2</sub>T<sub>x</sub> MXene nanosheets for 8 h in the dark resulted in >90% dispersion of the bacteria samples. Moreover, more than 95% of the DNA content was released from the bacteria cytosol.

# ■ MATERIALS AND METHODS

All reagents were analytical grade and were used without further purification.

**Preparation of Ti**<sub>3</sub>C<sub>2</sub>T<sub>x</sub> **MXene.** For preparation of Ti<sub>3</sub>C<sub>2</sub>T<sub>x</sub> powder, Ti<sub>3</sub>AlC<sub>2</sub> MAX powder (<38  $\mu$ m particle size) was etched using the synthesis method described in ref. First, 1 g of a LiF powder was dissolved in 20 mL of a 9 M hydrochloric acid solution over 5 min while stirring the solution at ambient temperature. Next, 1 g of the Ti<sub>3</sub>AlC<sub>2</sub> powder was added gradually to the solution for 10

min at ambient temperature while stirring the solution. To complete the reaction, the mixture was kept under stirring at 500 rpm at 35 °C for 24 h. To separate the supernatant from the Ti<sub>3</sub>C<sub>2</sub>T<sub>x</sub> sediment, 50 mL of DI water was added to the mixture followed by centrifuging at 3500 rpm for 5 min. Supernatant color was changed to dark green by repeating the washing step for 5-6 times (pH  $\sim$  6). After 1 h centrifuging, the sediment was separated followed by redispersing the sediment in DI water by vigorous shaking and centrifuging at 3500 rpm (2500g) for another 30 min. The supernatant containing large Ti<sub>3</sub>C<sub>2</sub>T<sub>x</sub> flakes in DI water was collected. Using a Celgard film (0.25 um pore size, 3501 Cated PP, Celgard), the sediment was filtered and dried under vacuum at room temperature to get multilayered Ti<sub>3</sub>C<sub>2</sub>T<sub>x</sub> powder. 0.08 g of the multilayered Ti<sub>3</sub>C<sub>2</sub>T<sub>x</sub> powder was dispersed in 50 mL of DI water and sealed under N2 blanketing. To obtain different flake sizes of Ti<sub>3</sub>C<sub>2</sub>T<sub>x</sub>, the sealed Ti<sub>3</sub>C<sub>2</sub>T<sub>x</sub> suspension was bath-sonicated (Branson 2510 Ultrasonic Cleaner, 100 W) at 20 °C

**Bacteria Strains.** The Gram-negative bacteria, *Escherichia coli* (*E. coli*, mc4100 strain, ATCC 35695) and Gram-positive bacteria, *Bacillus subtilis* (*B. subtilis*, Ehrenberg Cohn 168 strain, ATCC 23857) were cultivated on Lauria Broth agar (LB Broth with agar Lennox, Cat. No.: L2897, Sigma-Aldrich) medium plates at 37 °C for ~24 h and then stored at 4 °C for future use.

Bacteria Growth Measurements in the Presence of the **MXene Nanosheets.** To measure changes in the growth of *E. coli* and B. subtilis bacteria strains induced by various sizes of the MXene nanosheets, we performed the broth microdilution experiments.<sup>5</sup> Terrific broth (TB) culture media was made of 9.52 g of Terrific Broth (Cat. No.: T0918, Sigma-Aldrich) and 0.8 mL of glycerin (Cat. No.: G31-1, Fisher Scientific, U.S.A.) in 200 mL of distilled deionized (DI) water (Millipore, 18.2 M $\Omega$ .cm) and was autoclaved at 121  $^{\circ}$ C for 20 min. To obtain statistical results, the experiments were performed on three separate single-colony of each bacteria strain. A single-colony of bacteria was grown aerobically at 37 °C in 4 mL of TB media in a shaking flask at 150 rpm for about 6-7 h. One ml of each harvested bacteria was transferred to a UV-vis spectrometer to measure the optical density of the bacteria suspensions at 600 nm (i.e.,  $OD_{600}$ ). For each sample, a bacteria stock with a density of ca. 2  $\times$  10<sup>8</sup> cfu/ml was prepared (OD<sub>600</sub> = 0.1 is equivalent to 10<sup>8</sup> cfu/ml) to be used for the broth microdilution experiments. In a 96-well microtiter plate (flat-bottom), each bacteria sample with a final density of 108 cfu/ml in TB media was treated with 0.09, 0.35, 0.57, and 4.40  $\mu$ m MXene nanosheets with a final concentration of 100  $\mu$ g/ mL (i.e., MXene stock suspensions of 200 μg/mL were sonicated at 37 kHz for 10-15 min before use). The ratio of the MXene nanosheets to the bacteria was estimated to be 1 picogram MXene to one colony-forming unit bacteria (i.e., 1 pg/cfu). The last two wells in each series contained untreated bacteria (i.e., no MXene) and TB media (i.e., control). The 96-well plate was then placed on the shaker to allow bacteria grow aerobically at 37  $^{\circ}$ C at 150 rpm for ~18 h. To prevent the solvent evaporation in the wells, a DI water bath was placed on the shaker. To quantify the number of cultivated bacteria in each well, we made FC measurements using a BD Accuri C6 Flow Cytometer. Samples were incubated with 30  $\mu$ L of 33  $\mu$ M SYTO9 (Molecular Probes) for 15 min in the dark at room temperature (i.e., the final SYTO9 concentration in each well was 5  $\mu$ M). Samples were then placed on the FC stage for analysis. The FC analysis was performed with a medium fluid rate and 10  $\mu$ L of samples. The SYTO9 was illuminated with a 15 mW argon ion laser (488 nm) and the fluorescence signals were collected through the FL3 channel with the detection wavelengths of ≤670 nm. The SYTO9 fluorescence (FL3-H) and the forward angle scattering (FSC-H) signals were amplified with the logarithmic mode (i.e., histogram with logarithmic bin of 500) and shown in logarithmic scale. To reduce the effect of debris in the FC analysis, we set thresholds of 10,000 for FSC-H and 100 for side angle scattering (SSC-H) signals. To do single-cell analysis, we used FSC-A versus FSC-H counter plot to remove doublets from our calculations in which the doublets show a separate population toward higher FSC-A values (A and H stand for the area and height of the signals, respectively). The number of events

recorded for the 10  $\mu$ L samples from each well were 67 000  $\pm$  500 counts.

Bacteria Preparation for Viability Measurements. To measure the viability of E. coli and B. subtilis bacteria strains treated with various sizes of the MXene nanosheets (i.e., to investigate antibacterial activity of the nanosheets against the bacteria strains), we performed two complementary techniques; that is, the FC and the fluorescence imaging (FI). A discrete colony of each bacteria strain was grown aerobically at 37 °C in 50 mL of the TB solution in a shaking flask at 150 rpm for 8 h (i.e., at middle-to-late exponential phase). The harvested bacteria were centrifuged (i.e., 1500×g, 2 min, room temperature) and then washed twice with enough phosphate buffer saline (i.e.,  $1 \times PBS$ ; pH = 7.3) to remove waste and residual TB. For each washing step, we used a Rotamix (10101-RKVSD, ATR Inc.) at 20 rpm to suspend the pellet bacteria cells in 1×PBS with no biomechanical forces applied to the bacteria during the resuspensions. After the suspensions were washed twice with sufficient 1×PBS, the supernatant was removed, and the pellets were collected for preparing the E. coli and B. subtilis stock samples in 1×PBS with the cell density of  $\sim 2 \times 10^8$  cfu/ml.

Bacteria Viability Measurements Made Using the FC Technique. For each bacteria strain, the corresponding bacteria stock was exposed to a series of various sizes of MXene nanosheets (i.e., 0.09, 0.35, 0.57, and 4.40  $\mu$ m) with the final densities of 100  $\mu$ g/ mL MXene and 108 cfu/ml in a 96-well microtiter flat-bottom plate (i.e., MXene stock suspensions of 200  $\mu$ g/mL were sonicated at 37 kHz for 10-15 min before use). The ratio of MXene nanosheets to the bacteria was estimated to be ~1 picogram MXene to one colonyforming unit bacteria (i.e., 1 pg/cfu). The 96-well plate containing the untreated and treated bacteria samples were placed on the shaker at room temperature at 150 rpm for 3 or 8 h in the dark. To prevent the solvent evaporation in the wells, a DI water bath was placed on the shaker. To make viability measurements of the bacteria samples using the FC technique (i.e., BD Accuri C6 Flow Cytometer), the samples were incubated with 30  $\mu$ L of 33  $\mu$ M SYTO9 (Molecular Probes) for 15 min in the dark at room temperature (i.e., the final SYTO9 concentration in each well was 5  $\mu$ M). Samples were then placed on the FC stage for analysis. The FC analysis was performed with a medium fluid rate and limits of measuring 10  $\mu$ L of samples. The SYTO9 was illuminated with a 15 mW argon ion laser (488 nm), and the fluorescence signals were collected through the FL3 channel with the detection wavelengths of ≤670 nm. The SYTO9 fluorescence (FL3-H) and the forward angle scattering (FSC-H) signals were amplified with the logarithmic mode (i.e., histogram with logarithmic bin of 500) and shown in the logarithmic scale. To record both debris and bacteria populations in our FC analysis, we set the thresholds of 1000 for FSC-H and 10 for side-angle scattering (SSC-H) signals, respectively. To do single-cell analysis, we used a FSC-A vs FSC-H counter plot to remove doublets from our calculations, in which the doublets show a separate population toward higher FSC-A values (i.e., A and H stand for the area and height of the signals, respectively).

Bacteria Viability Measurements by Using the Fluorescence Imaging. In each fluorescence imaging experiment, the untreated and treated bacterial suspensions (see the previous section for details) were incubated with 5  $\mu$ M SYTO9 (Molecular Probes) and 20  $\mu$ M propidium iodide (PI, Sigma-Aldrich) for 15 min in the dark at room temperature. A 20  $\mu$ L aliquot of each sample was then added onto a microscope glass slide, enclosed by a glass coverslip, and mounted on the fluorescence microscope stage. Epi-fluorescence images of at least 15 field-of-view (FOV) were recorded for each glass slide (i.e., each sample) and more than 2000 cells were counted in each experiment. The SYTO9-stained bacteria (i.e., green) correspond to the live bacteria and the PI-stained bacteria (i.e., red) correspond to the dead bacteria.

Fluorescence Microscope Setup and Image Analysis. A Nikon ECLIPSE TE200 microscope with a  $40\times/0.60$  PlanFlour (Nikon) objective lens coupled to a digital image capture system (Hamamatsu C11440) was used to record images by the NIS Elements (ver. 4.20) software. An EXFO X-cite 120 Fluorescence Illuminator light source was used to excite the PI and SYTO9

molecules, and the red and green fluorescence emissions were recorded in epi-fluorescence configuration through appropriate filter cubes. Filter cubes had an excitation and detection wavelengths, respectively, centered at 560 and 630 nm for PI (Prod. No.: 49008, CHROMA) and 480 and 535 nm for SYTO9 molecules (Prod. No.: 49011, CHROMA). Image analysis was performed by using ImageJ software (National Institutes of Health, 1.43u). In a typical image analysis, the images recorded by the two filter cubes were stacked to show the SYTO9-stained and PI-stained bacteria in a single FOV.

## ASSOCIATED CONTENT

### Supporting Information

The Supporting Information is available free of charge on the ACS Publications website at DOI: 10.1021/acssuschemeng.8b03823.

Details on the interference of the MXene nanosheets with the bacteria cells, investigated by FC; and UV—vis spectra of the MXene suspensions, XPS spectra, and SEM images of the MXene (PDF)

#### AUTHOR INFORMATION

#### Corresponding Author

\*E-mail: soroushm@drexel.edu. Tel.: +1-215-895-1710.

#### ORCID 4

Ahmad Arabi Shamsabadi: 0000-0002-9726-2466 Mohammad Sharifian Gh.: 0000-0003-3867-1611

Babak Anasori: 0000-0002-1955-253X

## **Author Contributions**

 $\P$ (A.A.S., M.S.G.) These authors contributed equally to this work.

# Notes

The authors declare no competing financial interest.

# ACKNOWLEDGMENTS

The authors are grateful to Mohammad F. Kiani (Temple University) and the Department of Bioengineering at Temple University for providing access to the fluorescence microscope and the flow cytometer equipment, respectively. Ahmad Arabi Shamsabadi was partially supported by the U.S. National Science Foundation (NSF) under Grant No. CBET—1804285. Mohammad Sharifian Gh. was supported by the NSF Grant No. CHE-1465096. The authors express their thanks to Yury Gogotsi for his invaluable comments and support.

## ABBREVIATIONS

FC = flow cytometry

FI = fluorescence imaging

XRD = X-ray diffraction

CM = cytoplasmic membrane

PM = peptidoglycan mesh

PI = propidium iodide

E. coli = Escherichia coli B. subtilis = Bacillus subtilis

MoA = mode-of-action

2D = two-dimensional

GO = graphene oxide

rGO = reduced graphene oxide

Gram + = Gram - positive

Gram— = Gram-negative

ROS = reactive oxygen species

# REFERENCES

- (1) Percival, S. L.; Bowler, P. G.; Russell, D. Bacterial Resistance to Silver in Wound Care. J. Hosp. Infect. 2005, 60 (1), 1-7.
- (2) Silver; Phung, L. T.; Silver, G. Silver as Biocides in Burn and Wound Dressings and Bacterial Resistance to Silver Compounds. J. Ind. Microbiol. Biotechnol. 2006, 33 (7), 627-634.
- (3) Helms, M.; Vastrup, P.; Gerner-Smidt, P.; Mølbak, K. Excess Mortality Associated with Antimicrobial Drug-Resistant Salmonella Typhimurium. *Emerging Infect. Dis.* **2002**, 8 (5), 490–495.
- (4) World Health Organization (WHO). Antibacterial Agents in Clinical Development: An Analysis of the Antibacterial Clinical Development Pipeline, Including Tuberculosis; WHO: Geneva, Switzerland, 2017.
- (5) Hu, W.; Peng, C.; Luo, W.; Lv, M.; Li, X.; Li, D.; Huang, Q.; Fan, C. Graphene-Based Antibacterial Paper. ACS Nano 2010, 4 (7),
- (6) Liu, S.; Zeng, T. H.; Hofmann, M.; Burcombe, E.; Wei, J.; Jiang, R.; Kong, J.; Chen, Y. Antibacterial Activity of Graphite, Graphite Oxide, Graphene Oxide, and Reduced Graphene Oxide: Membrane and Oxidative Stress. ACS Nano 2011, 5 (9), 6971-6980.
- (7) Wu, M.-C.; Deokar, A. R.; Liao, J.-H.; Shih, P.-Y.; Ling, Y.-C. Graphene-Based Photothermal Agent for Rapid and Effective Killing of Bacteria. ACS Nano 2013, 7 (2), 1281-1290.
- (8) Chernousova, S.; Epple, M. Silver as Antibacterial Agent: Ion, Nanoparticle, and Metal. Angew. Chem., Int. Ed. 2013, 52 (6), 1636-1653.
- (9) Xiu, Z. M.; Zhang, Q. B.; Puppala, H. L.; Colvin, V. L.; Alvarez, P. J. J. Negligible Particle-Specific Antibacterial Activity of Silver Nanoparticles. Nano Lett. 2012, 12 (8), 4271-4275.
- (10) Tang, Q.; Liu, J.; Shrestha, L. K.; Ariga, K.; Ji, Q. Antibacterial Effect of Silver-Incorporated Flake-Shell Nanoparticles under Dual-Modality. ACS Appl. Mater. Interfaces 2016, 8 (29), 18922-18929.
- (11) Tan, P.; Li, Y. H.; Liu, X. Q.; Jiang, Y.; Sun, L. B. Core-Shell AgCl@SiO2 Nanoparticles: Ag(I)-Based Antibacterial Materials with Enhanced Stability. ACS Sustainable Chem. Eng. 2016, 4 (6), 3268-
- (12) Bing, W.; Chen, Z.; Sun, H.; Shi, P.; Gao, N.; Ren, J.; Qu, X. Visible-Light-Driven Enhanced Antibacterial and Biofilm Elimination Activity of Graphitic Carbon Nitride by Embedded Ag Nanoparticles. Nano Res. 2015, 8 (5), 1648-1658.
- (13) Dadashi Firouzjaei, M.; Arabi Shamsabadi, A.; Sharifian Gh., M.; Rahimpour, A.; Soroush, M. A Novel Nanocomposite with Superior Antibacterial Activity: A Silver-Based Metal Organic Framework Embellished with Graphene Oxide. Adv. Mater. Interfaces **2018**, 1701365, 1-10.
- (14) Ma, P.; Jiang, L.; Yu, M.; Dong, W.; Chen, M. Green Antibacterial Nanocomposites from Poly(Lactide)/Poly(Butylene Adipate-Co-Terephthalate)/Nanocrystal Cellulose-Silver Nanohybrids. ACS Sustainable Chem. Eng. 2016, 4 (12), 6417-6426.
- (15) Jin, C.; Liu, X.; Tan, L.; Cui, Z.; Yang, X.; Zheng, Y.; Yeung, K. W. K.; Chue, P. K.; Wu, S. Ag/AgBr-Loaded Mesoporous Silica for Rapid Sterilization and Promotion of Wound Healing. Biomater. Sci. **2018**, *6*, 1735–1744.
- (16) Yin, W.; Yu, J.; Lv, F.; Yan, L.; Zheng, L. R.; Gu, Z.; Zhao, Y. Functionalized Nano-MoS2with Peroxidase Catalytic and Near-Infrared Photothermal Activities for Safe and Synergetic Wound Antibacterial Applications. ACS Nano 2016, 10 (12), 11000-11011.
- (17) Cao, F.; Ju, E.; Zhang, Y.; Wang, Z.; Liu, C.; Li, W.; Huang, Y.; Dong, K.; Ren, J.; Qu, X. An Efficient and Benign Antimicrobial Depot Based on Silver-Infused MoS2. ACS Nano 2017, 11 (5), 4651-4659.
- (18) Ge, L.; Xu, Y.; Li, X.; Yuan, L.; Tan, H.; Li, D.; Mu, C. Fabrication of Antibacterial Collagen-Based Composite Wound Dressing. ACS Sustainable Chem. Eng. 2018, 6 (7), 9153-9166.
- (19) Mao, C.; Xiang, Y.; Liu, X.; Cui, Z.; Yang, X.; Yeung, K. W. K.; Pan, H.; Wang, X.; Chu, P. K.; Wu, S. Photo-Inspired Antibacterial Activity and Wound Healing Acceleration by Hydrogel Embedded with Ag/Ag@AgCl/ZnO Nanostructures. ACS Nano 2017, 11 (9), 9010-9021.

- (20) Perreault, F.; Tousley, M. E.; Elimelech, M. Thin-Film Composite Polyamide Membranes Functionalized with Biocidal Graphene Oxide Nanosheets. Environ. Sci. Technol. Lett. 2014, 1 (1), 71-76.
- (21) Zirehpour, A.; Rahimpour, A.; Arabi Shamsabadi, A.; Sharifian Gh., M.; Soroush, M. Mitigation of Thin-Film Composite Membrane Biofouling via Immobilizing Nano-Sized Biocidal Reservoirs in the Membrane Active Layer. Environ. Sci. Technol. 2017, 51 (10), 5511-
- (22) Durán, N.; Marcato, P. D.; De Souza, G. I. H.; Alves, O. L.; Esposito, E. Antibacterial Effect of Silver Nanoparticles Produced by Fungal Process on Textile Fabrics and Their Effluent Treatment. J. Biomed. Nanotechnol. 2007, 3 (2), 203-208.
- (23) Shi, L.; Chen, J.; Teng, L.; Wang, L.; Zhu, G.; Liu, S.; Luo, Z.; Shi, X.; Wang, Y.; Ren, L. The Antibacterial Applications of Graphene and Its Derivatives. Small 2016, 12 (31), 4165-4184.
- (24) Xu, W.; Xie, W.; Huang, X.; Chen, X.; Huang, N.; Wang, X.; Liu, J. The Graphene Oxide and Chitosan Biopolymer Loads TiO2 for Antibacterial and Preservative Research. Food Chem. 2017, 221, 267-277.
- (25) Kim, T. I.; Kwon, B.; Yoon, J.; Park, I. J.; Bang, G. S.; Park, Y. K.; Seo, Y. S.; Choi, S. Y. Antibacterial Activities of Graphene Oxide-Molybdenum Disulfide Nanocomposite Films. ACS Appl. Mater. Interfaces 2017, 9 (9), 7908-7917.
- (26) Gu, Z.; Yang, Z.; Kang, S. G.; Yang, J. R.; Luo, J.; Zhou, R. Robust Denaturation of Villin Headpiece by MoS2Nanosheet: Potential Molecular Origin of the Nanotoxicity. Sci. Rep. 2016, 6 (1), 1-8.
- (27) Choudhary, P.; Parandhaman, T.; Ramalingam, B.; Duraipandy, N.; Kiran, M. S.; Das, S. K. Fabrication of Nontoxic Reduced Graphene Oxide Protein Nanoframework as Sustained Antimicrobial Coating for Biomedical Application. ACS Appl. Mater. Interfaces 2017, 9 (44), 38255-38269.
- (28) Liao, K. H.; Lin, Y. S.; MacOsko, C. W.; Haynes, C. L. Cytotoxicity of Graphene Oxide and Graphene in Human Erythrocytes and Skin Fibroblasts. ACS Appl. Mater. Interfaces 2011, 3 (7), 2607-2615.
- (29) Jastrzębska, A. M.; Szuplewska, A.; Wojciechowski, T.; Chudy, M.; Ziemkowska, W.; Chlubny, L.; Rozmysłowska, A.; Olszyna, A. In Vitro Studies on Cytotoxicity of Delaminated Ti<sub>3</sub>C<sub>2</sub>T<sub>x</sub> MXene. J. Hazard. Mater. 2017, 339, 1-8.
- (30) Xie, X.; Mao, C.; Liu, X.; Zhang, Y.; Cui, Z.; Yang, X.; Yeung, K. W. K.; Pan, H.; Chu, P. K.; Wu, S. Synergistic Bacteria Killing through Photodynamic and Physical Actions of Graphene Oxide/Ag/ Collagen Coating. ACS Appl. Mater. Interfaces 2017, 9 (31), 26417-
- (31) Mao, C.; Xiang, Y.; Liu, X.; Cui, Z.; Yang, X.; Li, Z.; Zhu, S.; Zheng, Y.; Yeung, K. W. K.; Wu, S. Repeatable Photodynamic Therapy with Triggered Signaling Pathways of Fibroblast Cell Proliferation and Differentiation To Promote Bacteria-Accompanied Wound Healing. ACS Nano 2018, 12 (2), 1747-1759.
- (32) Barbolina, I.; Woods, C. R.; Lozano, N.; Kostarelos, K.; Novoselov, K. S.; Roberts, I. S. Purity of Graphene Oxide Determines Its Antibacterial Activity. 2D Mater. 2016, 3 (2), 025025.
- (33) Nanda, S. S.; Yi, D. K.; Kim, K. Study of Antibacterial Mechanism of Graphene Oxide Using Raman Spectroscopy. Sci. Rep. **2016**, 6 (1), 1–12.
- (34) Akhavan, O.; Ghaderi, E. Toxicity of Graphene and Graphene Oxide Nanowalls Against Bacteria. ACS Nano 2010, 4 (10), 5731-
- (35) Akhavan, O.; Ghaderi, E. Escherichia Coli Bacteria Reduce Graphene Oxide to Bactericidal Graphene in a Self-Limiting Manner. Carbon 2012, 50 (5), 1853-1860.
- (36) Akhavan, O.; Ghaderi, E.; Esfandiar, A. Wrapping Bacteria by Graphene Nanosheets for Isolation from Environment, Reactivation by Sonication, and Inactivation by Near-Infrared Irradiation. J. Phys. Chem. B 2011, 115 (19), 6279-6288.

- (37) Perreault, F.; De Faria, A. F.; Nejati, S.; Elimelech, M. Antimicrobial Properties of Graphene Oxide Nanosheets: Why Size Matters. ACS Nano 2015, 9 (7), 7226–7236.
- (38) Luo, J.; Lai, J.; Zhang, N.; Liu, Y.; Liu, R.; Liu, X. Tannic Acid Induced Self-Assembly of Three-Dimensional Graphene with Good Adsorption and Antibacterial Properties. *ACS Sustainable Chem. Eng.* **2016**, *4* (3), 1404–1413.
- (39) Sun, W.; Wu, F.-G. Two-Dimensional Materials for Antimicrobial Applications: Graphene Materials and Beyond. *Chem.*—*Asian J.* **2018**, DOI: 10.1002/asia.201800851.
- (40) Li, Y.; Liu, X.; Tan, L.; Cui, Z.; Yang, X.; Zheng, Y.; Yeung, K. W. K.; Chu, P. K.; Wu, S. Rapid Sterilization and Accelerated Wound Healing Using Zn2+ and Graphene Oxide Modified G-C3N4 under Dual Light Irradiation. *Adv. Funct. Mater.* **2018**, 28 (30), 1800299.
- (41) Yang, X.; Li, J.; Liang, T.; Ma, C.; Zhang, Y.; Chen, H.; Hanagata, N.; Su, H.; Xu, M. Antibacterial Activity of Two-Dimensional MoS2 Sheets. *Nanoscale* **2014**, *6* (17), 10126–10133.
- (42) Alimohammadi, F.; Sharifian Gh., M.; Attanayake, N. H.; Thenuwara, A. C.; Gogotsi, Y.; Anasori, B.; Strongin, D. R. Antimicrobial Properties of 2D MnO2 and MoS2 Nanomaterials Supported on Graphene and Ti<sub>3</sub>C<sub>2</sub>T<sub>x</sub> MXene. *Langmuir* **2018**, 34 (24), 7192–200.
- (43) Feng, Z.; Liu, X.; Tan, L.; Cui, Z.; Yang, X.; Li, Z.; Zheng, Y.; Yeung, K. W. K.; Wu, S. Electrophoretic Deposited Stable Chitosan@ MoS2 Coating with Rapid In Situ Bacteria-Killing Ability under Dual-Light Irradiation. *Small* **2018**, *14* (21), 1704347.
- (44) Pandit, S.; Karunakaran, S.; Boda, S. K.; Basu, B.; De, M. High Antibacterial Activity of Functionalized Chemically Exfoliated MoS2. *ACS Appl. Mater. Interfaces* **2016**, *8* (46), 31567–31573.
- (45) Xie, X.; Mao, C.; Liu, X.; Tan, L.; Cui, Z.; Yang, X.; Zhu, S.; Li, Z.; Yuan, X.; Zheng, Y.; et al. Tuning the Bandgap of Photo-Sensitive Polydopamine/Ag3PO4/Graphene Oxide Coating for Rapid, Noninvasive Disinfection of Implants. ACS Cent. Sci. 2018, 4 (6), 724–738.
- (46) Rasool, K.; Mahmoud, K. A.; Johnson, D. J.; Helal, M.; Berdiyorov, G. R.; Gogotsi, Y. Efficient Antibacterial Membrane Based on Two-Dimensional  ${\rm Ti_3C_2T_x}$  (MXene) Nanosheets. *Sci. Rep.* **2017**. 7 (1), 1598.
- (47) Rasool, K.; Helal, M.; Ali, A.; Ren, C. E.; Gogotsi, Y.; Mahmoud, K. A. Antibacterial Activity of Ti<sub>3</sub>C<sub>2</sub>T<sub>x</sub> MXene. *ACS Nano* **2016**, *10* (3), 3674–3684.
- (48) Zheng, K.; Setyawati, M. I.; Leong, D. T.; Xie, J. Antimicrobial Gold Nanoclusters. *ACS Nano* **2017**, *11* (7), 6904–6910.
- (49) Tan, L.; Li, J.; Liu, X.; Cui, Z.; Yang, X.; Yeung, K. W. K.; Pan, H.; Zheng, Y.; Wang, X.; Wu, S. In Situ Disinfection through Photoinspired Radical Oxygen Species Storage and Thermal-Triggered Release from Black Phosphorous with Strengthened Chemical Stability. *Small* **2018**, *14*, 1703197.
- (50) Wiegand, I.; Hilpert, K.; Hancock, R. E. W. Agar and Broth Dilution Methods to Determine the Minimal Inhibitory Concentration (MIC) of Antimicrobial Substances. *Nat. Protoc.* **2008**, *3* (2), 163–175.
- (51) Jepras, R. I.; Carter, J.; Pearson, S. C.; Paul, F. E.; Wilkinson, M. J. Development of a Robust Flow Cytometric Assay for Determining Numbers of Viable Bacteria. *Appl. Environ. Microbiol.* **1995**, *61* (7), 2696–2701.
- (52) Lopez-Amoros, R.; Comas, J.; Vives-Rego, J. Flow Cytometric Assessment of Escherichia Coli and Salmonella Typhimurium Starvation-Survival in Seawater Using Rhodamine 123, Propidium Iodide, and Oxonol. *Appl. Environ. Microbiol.* **1995**, *61* (7), 2521–2526.
- (53) Löpez-Amorós, R.; Castel, S.; Comas-Riu, J.; Vives-Rego, J. Assessment of E. Coli and Salmonella Viability and Starvation by Confocal Laser Microscopy and Flow Cytometry Using Rhodamine 123, DiBAC4(3), Propidium Iodide, and CTC. Cytometry 1997, 29 (1997), 298–305.
- (54) Madigan, M. T.; Martinko, J. M.; Stahl, D. A.; Clark, D. P. *Brock Biology of Microorganisms*, 13th ed.; Pearson Education, Inc.: San Francisco, CA, 2012.

- (55) Koch, A. L. Some Calculations on the Turbidity of Mitochondria and Bacteria. *Biochim. Biophys. Acta* **1961**, *51*, 429–441.
- (56) Koch, A. L. Theory of the Angular Dependence of Light Scattered by Bacteria and Similar-Sized Biological Objects. *J. Theor. Biol.* **1968**, *18* (1), 133–156.
- (57) Koch, A. L. Turbidity Measurements of Bacterial Cultures in Some Available Commercial Instruments. *Anal. Biochem.* **1970**, 38 (1), 252–259.
- (58) Scott, M.; Gunderson, C. W.; Mateescu, E. M.; Zhang, Z.; Hwa, T. Interdependence of Cell Growth and Gene Expression: Origins and Consequences. *Science* **2010**, 330, 1099–1102.
- (59) Klumpp, S.; Zhang, Z.; Hwa, T. Growth Rate-Dependent Global Effects on Gene Expression in Bacteria. *Cell* **2009**, *139*, 1366–1375.
- (60) Neidhardt, F. C. Escherichia Coli and Salmonella: Cellular and Molecular Biology, 2nd ed.; American Society for Microbiology, 1996.
- (61) Levin, B. R.; Udekwu, K. I. Population Dynamics of Antibiotic Treatment: A Mathematical Model and Hypotheses for Time-Kill and Continuous-Culture Experiments. *Antimicrob. Agents Chemother.* **2010**, *54* (8), 3414–3426.
- (62) Holowachuk, S. A.; Bal'a, M. F.; Buddington, R. K. A Kinetic Microplate Method for Quantifying the Antibacterial Properties of Biological Fluids. *J. Microbiol. Methods* **2003**, 55 (2), 441–446.
- (63) Bollenbach, T.; Quan, S.; Chait, R.; Kishony, R. Nonoptimal Microbial Response to Antibiotics Underlies Suppressive Drug Interactions. *Cell* **2009**, *139*, 707–718.
- (64) Andrews, J. M. Determination of Minimum Inhibitory Concentrations. *J. Antimicrob. Chemother.* **2001**, *48*, 5–16.
- (65) Theophel, K.; Schacht, V. J.; Schlüter, M.; Schnell, S.; Stingu, C. S.; Schaumann, R.; Bunge, M. The Importance of Growth Kinetic Analysis in Determining Bacterial Susceptibility Against Antibiotics and Silver Nanoparticles. *Front. Microbiol.* **2014**, *5* (NOV), 544.
- (66) Tas, J.; Westerneng, G. Fundamental Aspects of the Interaction of Propidium Diiodide with Nuclei Acids Studied in a Model System of Polyacrylamide Films. *J. Histochem. Cytochem.* **1981**, 29, 929–936.
- (67) Hudson, B.; Upholt, W. B.; Devinny, J.; Vinograd, J. The Use of an Ethidium Analogue in the Dye-Buoyant Density Procedure for the Isolation of Closed Circular DNA: The Variation of the Superhelix Density of Mitochondrial DNA. *Proc. Natl. Acad. Sci. U. S. A.* 1969, 62, 813–820.
- (68) Grossman, L. I.; Watson, R.; Vinograd, J. Restricted Uptake of Ethidium Bromide and Propidium Diiodide by Denatured Closed Circular DNA in Buoyant Cesium Chloride. *J. Mol. Biol.* **1974**, *86*, 271–283
- (69) Yeh, C. J. G.; Hsi, B.-L.; Faulk, W. P. Propidium Iodide as a Nuclear Marker in Immunofluorescence. II. Use with Cellular Identification and Viability Studies. *J. Immunol. Methods* **1981**, 43, 269–275.
- (70) Banning, N.; Toze, S.; Mee, B. J. Escherichia Coli Survival in Groundwater and Effluent Measured Using a Combination of Propidium Iodide and the Green Fluorescent Protein. *J. Appl. Microbiol.* **2002**, 93 (1), 69–76.
- (71) Williams, S. C.; Hong, Y.; Danavall, D. C.; Howard-Jones, M. H.; Gibson, D.; Frischer, M. E.; Verity, P. G. Distinguishing between Living and Nonliving Bacteria: Evaluation of the Vital Stain Propidium Iodide and Its Combined Use with Molecular Probes in Aquatic Samples. *J. Microbiol. Methods* 1998, 32, 225–236.
- (72) Godlewska, R.; Wiśniewska, K.; Pietras, Z.; Jagusztyn-Krynicka, E. K. Peptidoglycan-Associated Lipoprotein (Pal) of Gram-Negative Bacteria: Function, Structure, Role in Pathogenesis and Potential Application in Immunoprophylaxis. *FEMS Microbiol. Lett.* **2009**, 298 (1), 1–11.
- (73) Popescu, A.; Doyle, R. J. The Gram Stain after More than a Century. Biotech. Histochem. 1996, 71 (3), 145-151.
- (74) Büttner, K.; Bernhardt, J.; Scharf, C.; Schmid, R.; Mäder, U.; Eymann, C.; Antelmann, H.; Völker, A.; Völker, U.; Hecker, M. A Comprehensive Two-Dimensional Map of Cytosolic Proteins of Bacillus Subtilis. *Electrophoresis* **2001**, *22*, 2908–2935.

- (75) Beveridge, T. J. Ultrastructure, Chemistry, and Function of the Bacterial Wall. *Int. Rev. Cytol.* **1981**, *72*, 229–317.
- (76) Harden, V. P.; Harris, J. O. The Isoelectric Point of Bacterial Cells. J. Bacteriol. 1953, 65 (2), 198–202.
- (77) Vollmer, W.; Blanot, D.; de Pedro, M. A. Peptidoglycan Structure and Architecture. *FEMS Microbiol. Rev.* **2008**, 32 (2), 149–167.
- (78) Tu, Y.; Lv, M.; Xiu, P.; Huynh, T.; Zhang, M.; Castelli, M.; Liu, Z.; Huang, Q.; Fan, C.; Fang, H.; Zhou, R. Destructive Extraction of Phospholipids from Escherichia Coli Membranes by Graphene Nanosheets. *Nat. Nanotechnol.* **2013**, *8* (12), 968.
- (79) Andón, F. T.; Fadeel, B. Programmed Cell Death: Molecular Mechanisms and Implications for Safety Assessment of Nanomaterials. *Acc. Chem. Res.* **2013**, 46 (3), 733–742.
- (80) Nasrallah, G. K.; Al-Asmakh, M.; Rasool, K.; Mahmoud, K. A. Ecotoxicological Assessment of  ${\rm Ti_3C_2T_x}$  (MXene) Using a Zebrafish Embryo Model. *Environ. Sci.: Nano* **2018**, *5*, 1002–1011.
- (81) Li, J.; Tan, L.; Liu, X.; Cui, Z.; Yang, X.; Yeung, K. W. K.; Chu, P. K.; Wu, S. Balancing Bacteria—Osteoblast Competition through Selective Physical Puncture and Biofunctionalization of ZnO/Polydopamine/Arginine-Glycine-Aspartic Acid-Cysteine Nanorods. *ACS Nano* 2017, 11 (11), 11250—11263.
- (82) Tan, L.; Li, J.; Liu, X.; Cui, Z.; Yang, X.; Zhu, S.; Li, Z.; Yuan, X.; Zheng, Y.; Yeung, K. W. K.; et al. Rapid Biofilm Eradication on Bone Implants Using Red Phosphorus and Near-Infrared Light. *Adv. Mater.* **2018**, 30 (31), e1801808.
- (83) Alhabeb, M.; Maleski, K.; Anasori, B.; Lelyukh, P.; Clark, L.; Sin, S.; Gogotsi, Y. Guidelines for Synthesis and Processing of 2d Titanium Carbide (Ti<sub>3</sub>C<sub>2</sub>T<sub>x</sub> Mxene). *Chem. Mater.* **2017**, 29, 7633–7644.